Proceedings of the
Annual Stability Conference
Structural Stability Research Council
San Antonio, Texas, March 21-24, 2017

Design Method for Columns with Intermediate Elastic Torsional Restraint

Hannah B. Blum[1], Kim J.R. Rasmussen[2]

Abstract

Cold-formed steel haunched portal frames are popular structures in industrial and housing applications. They are mostly used as sheds, garages, and shelters, and are common in rural areas. Cold-formed steel portal frames with spans of up to 30 m (100 ft) are now being constructed in Australia. As these large structures are fairly new to the market, there is limited data on their performance and inadequate design guidance and recommendations. In the specific frame system analyzed herein, the column is partially restrained against twist rotation at an intermediate point where the knee brace joining the rafter and column is connected, and is otherwise unbraced. Current design guidelines do not directly account for the restraint provided by the knee connection and require the determination of the member effective length. Due to the variations of the column base stiffness and rotational restraint of the knee connection, the column effective length is difficult to quantify. Therefore, a new design method is proposed in this paper which eliminates the need to determine the effective length. The design capacity is calculated using the Direct Strength Method with inputs from a column buckling energy analysis. Internal actions are determined using a calibrated beam finite element model with notional horizontal forces, and the interaction equation involving bending and compression is utilized to determine the column strength. A reliability check is completed and the results compared to experimental frame ultimate loads. It is shown that the frame strength determined from the design method presented herein is a suitable method for the design of columns with an intermediate elastic torsional restraint in haunched portal frames.

1. Background

Cold-formed steel haunched portal frames are prevalent structures in industrial and housing uses, especially in rural regions of Australia. There is a demand for the construction of larger spans; however there is minimal test data on the strength and performance of larger span frames. Frames may have braced columns where girts are required for cladding, or unbraced columns when the frames are mainly used for shelters over large areas. For larger spans, a knee brace is required to transfer the large bending moment from the rafters to the columns. The knee brace to column connection, as shown in Fig. 1, creates an intermediate elastic torsional restraint on the unbraced column. Although some guidelines exist for cold-formed steel portal frames (ASI 2014; ECCS 2008), there is no direct guidance on how to account for the effects of the knee

[1] Associate Lecturer, University of Sydney, <hannah.blum@sydney.edu.au>
[2] Professor and Associate Dean Research, University of Sydney, <kim.rasmussen@sydney.edu.au>

connection on frame performance. Additionally, effective lengths are required in the design calculations; however due to the semi-rigidity of the column bases and the effect of the knee connection, an appropriate effective length is difficult to quantify.

An experimental program was carried out on a series of 13.6 m (44.6 ft) span portal frame systems, the layout of which is shown in Fig. 2. The program consisted of 8 tests of frames having unbraced columns, with variations in the knee connection sizing, and with applied vertical loads only, or applied horizontal and vertical loads. The experiments provided data on the ultimate loads of the frames, and on frame overall behavior including failure modes. Column base stiffness was also measured, as was the contribution of sleeve stiffeners, and the exact material and section properties were measured for use in calibrated finite element models. Further details of the experimental program can be found elsewhere (Blum 2017; Blum & Rasmussen 2016d). The data from the experiments is used to validate the design method presented herein. Methods to determine both the column capacity and the internal actions of the frame are discussed, and comparisons between design and experimental ultimate strengths are presented.

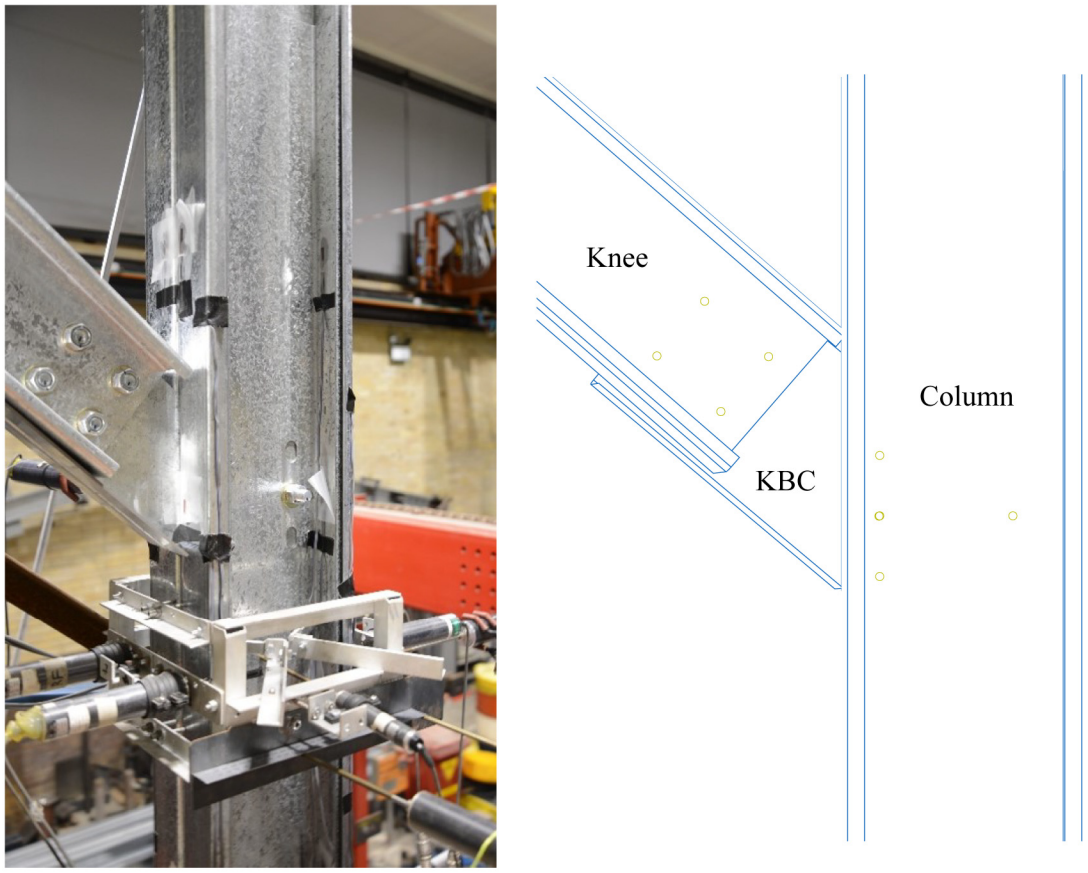

(a) (b)

Figure 1: Knee to column connection (a) experimental setup with instrumentation, and (b) drawing from front view

Figure 2: Frame experimental setup

2. Column Capacity

The nominal member capacity of a member in compression and the nominal member moment capacity of a member subject to bending can be calculated through use of the Direct Strength Method (DSM). This method is provided in various design codes such as in Section 7 of AS 4600 (AS/NZS 4600 2005) and in Appendix 1 of AISI (AISI-S100-12 2012). The DSM is a method applicable to cold-formed steel compression members and members subject to bending for all pre-qualified sections stated in the design codes. The DSM facilitates the calculations of the nominal member capacity of a member in compression and the nominal member moment capacity, separately. Further details can be found elsewhere (Schafer 2006).

Nominal member design strengths are calculated for local, global, and distortional buckling under given loading and support conditions, of which the minimum is the member design strength. In order to calculate the global buckling loads, the elastic lateral-torsional buckling moment and elastic member buckling load must be determined. A method to determine the elastic buckling loads and a subsequent design procedure to calculate frame capacity is presented herein.

2.1 Bending

For the design of members subject to bending, the elastic lateral-torsional moment, M_o, is required. This is typically calculated in Section 3 of AS/NZS 4600, where M_o is the elastic buckling moment. For doubly symmetric sections bent about the x-axis, the elastic buckling moment is defined in Eq. 1, where C_b is the coefficient to account for the moment distribution in

the unbraced segment, A is the area of the full cross-section, r_{ol} is the polar radius of gyration of the cross-section about the shear center, f_{oy} is the elastic buckling stress in an axially loaded compression member for flexural buckling about the y-axis (as defined in Eq. 2), and f_{oz} is the elastic buckling stress in an axially loaded compression member for torsional buckling, as defined in Eq. 3. The elastic buckling stresses (f_{oy} and f_{oz}) are dependent on the material properties of Young's modulus (E) and shear modulus (G), the geometric properties A, r_{ol}, the radius of gyration about the y-axis (r_y), the torsion constant (J), and the warping constant (I_w), and the effective lengths for buckling about the y-axis (l_{ey}), and for twisting, (l_{ez}).

$$M_o = C_b A r_{ol} \sqrt{f_{oy} f_{oz}} \tag{1}$$

$$f_{oy} = \frac{\pi^2 E}{\left(l_{ey}/r_y\right)^2} \tag{2}$$

$$f_{oz} = \frac{GJ}{Ar_{ol}^2}\left(1 + \frac{\pi^2 E I_w}{GJ l_{ez}^2}\right) \tag{3}$$

The effective lengths of the column, l_{ey} and l_{ez}, are unknown as it is difficult to quantify the effects of the knee connection on column effective lengths. Additionally, with this method, modifications to the knee brace connection (KBC), such as using a thicker bracket to connect the knee brace to the column, could only be reflected in modifying the effective lengths. Design codes currently do not explicitly state how to incorporate the effects of the intermediate torsional restraint of the knee to column connection on the calculated effective lengths of the column.

Previous work has been completed on the calculation of buckling loads of columns with an intermediate elastic torsional restraint through an energy method approach (Blum & Rasmussen 2016a), where the column buckling load can be determined by minimizing the total energy of the column. The total energy of the column is the sum of the flexural, torsional, and warping strain energies stored in the column, the potential energy associated with the internal axial force N and bending moment M, the work done by the forces acting at the knee brace connection, and the spring energy stored in the KBC connection plate. As the knee brace moves out of plane of the frame, it causes the column to move laterally (v-direction) and twist (ϕ-direction), and acts as a directed load (Ings & Trahair 1987). Therefore, the work at the knee connection is the forces at the knee connection (F_v and F_u) multiplied with the displacements through which they act (v_{kc} and u_{kc}), as given in Eq. 4 where v_k and ϕ_k are the lateral displacement of the column and the column twist, respectively, at the location of the knee connection, d_s is the distance from the load application point to the shear center of the column, θ is the angle between the column and the knee brace, L_k is the length of the knee brace, and F is the force in the knee brace. Further derivations are given elsewhere (Blum & Rasmussen 2016a).

$$W_k = F_v v_{kc} + F_u u_{kc} = F\left(v_k + \phi_k d_s\right)^2 / L_k + 1/2\, F \sin\theta\, \phi_k^2\, d_s \tag{4}$$

The knee brace to column connection plate acts as a torsional spring to the column and helps to restrain the column against twist at the connection. The strain energy stored in the plate is given

in Eq. 5, where k_ϕ is the torsional stiffness of the plate and $\Delta\theta_{kc}$ is the total rotation of the plate. The plate stiffness is calculated using plate bending theory (Timoshenko & Gere 1989) where the plate is bent in only one direction, and as the KBC bracket is composed to two plates bolted together, the plate stiffness is double that of a single plate. The double-plate stiffness is calculated in Eq. 6, where h is the plate height, b is the plate width, E is Young's modulus, t_k is the thickness of a single KBC connection plate, v is Poisson's ratio, and D is the plate flexural rigidity. The total rotation of the plate, Eq. 7, is the sum of the column rotation at the knee, ϕ_k, and the rotation due to the knee brace movement.

$$U_s = 1/2\, k_\phi \left(\Delta\theta_{kc}\right)^2 \tag{5}$$

$$k_\phi = 2\left[\frac{E\, t_k^{\,3}}{12\left(1-\nu^2\right)}\right]\left(h/b\right) \tag{6}$$

$$\Delta\theta_{kc} = \phi_k + v_{kc}/L_k \sin\theta \tag{7}$$

Combining these energy components yields the total energy of the column, as given in Eq. 8. Column displacement fields for v and ϕ must be quantified. Displacements at various locations along the length of the column were measured during experiments (Blum & Rasmussen 2016d) and the resulting approximate displacement functions of the column are given in Eqs. 9 and 10. As the displaced shape was measured from the experiments, the effects of the column semi-rigid base connections are inherently included. The column buckling load can be solved by minimizing the total energy of the column, $\delta V_T = 0$, and for non-trivial solutions, Eq. 11 must be solved. Measured dimensions, thicknesses, and material properties of the column and KBC brackets were used in the analysis, as were internal forces N and M distributions from a validated finite element beam model, which is described elsewhere (Blum & Rasmussen 2016a). Results from the energy analysis are within a 10% overestimation of the experimental ultimate loads (columns failed by elastic lateral-torsional buckling) indicating that the energy method approach was a viable method for determining column buckling loads for this type of structure (Blum 2017).

$$\begin{aligned} V_T = {} & \frac{1}{2}\int_0^L \left(EI_y v''^2 + EI_w \phi''^2 + GJ\phi'^2\right)dz \; + \frac{1}{2}\int_0^L M\left(2\phi v''\right)dz - \frac{1}{2}\int_0^L N\left(v'^2 + r_2^2\phi'^2\right)dz \\ & - F\left(v_k + \phi_k d_s\right)^2 / L_k + 1/2\, F \sin\theta\, \phi_k^2\, d_s + 1/2\, k_\phi \left(\Delta\theta_{kc}\right)^2 \end{aligned} \tag{8}$$

$$v = A_v\left(\sin\left(\frac{\pi z}{L}\right) - 0.2 * \sin\left(\frac{2\pi z}{L}\right)\right) \tag{9}$$

$$\phi = A_\phi\left(\sin\left(\frac{\pi z}{L}\right) - 0.2 * \sin\left(\frac{2\pi z}{L}\right)\right) \tag{10}$$

$$\frac{\partial V_T}{\partial A_V} = \frac{\partial V_T}{\partial A_\varphi} = 0 \tag{11}$$

The elastic column buckling load, P_{cr}, determined from the energy analysis, is the axial load applied to the column at buckling. The column buckling is dominated by the bending moment, and therefore the maximum bending moment in the column when $P=P_{cr}$ is the critical bending moment, M_{cr}, which is the elastic buckling moment of the column. The relationship between P_{cr} and M_{cr} is described elsewhere (Blum & Rasmussen 2016a). Therefore, in lieu of calculating M_o as shown in Eq. 1 from Section 3 of AS/NZS 4600, the energy analysis can be utilized, and therefore $M_o = M_{cr}$. This method eliminates the need to determine effective lengths of the column, and considers the effects of the torsional spring at the knee connection through the geometric and material properties of the KBC connection bracket in Eq. 6, as well as incorporates the semi-rigidity of the column base connection.

2.2 Compression

For the design of members subject to compression, N_{oc} must be determined, as given in Eq. 12, where f_{oc} is the least of the elastic flexural, torsional, and flexural-torsional buckling stresses, and is typically calculated in Section 3 of AS/NZS 4600. For doubly-symmetric sections not subject to flexural or flexural-torsional buckling, f_{oc} is taken as the minimum of f_{ox}, as given in Eq. 13, and f_{oy}. Therefore, the effective lengths l_{ex}, and l_{ey} are required. As these effective lengths are difficult to quantify, it would be difficult to accurately determine the elastic compressive buckling load. In the energy method approach to determine column buckling, the critical column axial load, P_{cr} was determined considering the simultaneous presence of axial force and bending moment, which resulted in the critical compression force, P_{cr}, and bending moment, M_{cr} in the column. However, if bending and compression capacities are considered separately, the value of P_{cr} thus calculated is not the critical buckling load of the column for compression only.

$$N_{oc} = A f_{oc} \tag{12}$$

$$f_{ox} = \frac{\pi^2 E}{\left(l_{ex}/r_x\right)^2} \tag{13}$$

The column elastic critical buckling load can be determined through an Euler buckling analysis, as given in Eq. 14, where L is the length of the column and k is the effective length factor. A buckling analysis was completed in MASTAN2 (McGuire et al. 2000) with a base spring applied to the column with an average stiffness as determined from the experiments, and with the measured elastic modulus and cross-section dimensions (Blum & Rasmussen 2016c). The Euler buckling load was calculated to be $(P_{cr})_{Euler}$=765 kN (172 kip) with an effective length factor k=0.936. Therefore, instead of calculating N_{oc} as given in Eq. (12) where f_{oc} is calculated according to Section 3 of AS/NZS 4600, $N_{oc} = (P_{cr})_{Euler}$ can be utilized.

$$\left(P_{cr}\right)_{Euler} = \frac{\pi^2 E I_x}{k^2 L^2} \tag{14}$$

2.3 Capacity Results

Now that the critical elastic lateral-torsional buckling moment (M_{cr}) and critical elastic flexural column buckling load ($N_{oc} = (P_{cr})_{Euler}$) have been determined, the Direct Strength Method can be employed to calculate the capacity of the column in bending and in compression.

For the capacity in bending, four input values are needed: the elastic lateral-torsional buckling moment M_o, the nominal section moment capacity M_y as given in Eq. 15 where Z_f is the full section modulus of the extreme fiber at first yield and f_y is the yield stress, and the elastic buckling moments, M_{ol} and M_{od}, for local and distortional buckling, respectively. M_{ol} and M_{od} are given in Eqs. 16 and 17, where the local and distortional buckling stresses, f_{ol} and f_{od}, can be determined through a finite strip analysis with applied bending stresses on the column cross-section through software such as CUFSM (Li & Schafer 2010) and ThinWall (Papangelis & Hancock 1995). Further details can be found elsewhere (Schafer 2006). The section modulus Z_f is calculated from the measured column dimensions, and f_y is taken as the measured yield stress from the experiments (Blum & Rasmussen 2016c).

$$M_y = Z_f f_y \tag{15}$$

$$M_{ol} = Z_f f_{ol} \tag{16}$$

$$M_{od} = Z_f f_{od} \tag{17}$$

The critical bending moments, M_{cr}, for the columns in each experiment were calculated using the energy analysis described previously and are given in Table 1. Following the Direct Strength Method for M_o=M_{cr} and the values determined for f_{ol} and f_{od} from a finite strip analysis with the measured column dimensions, the member moment capacity, M_b, is calculated for each column and is given in Table 1. M_b is the minimum of the member moment capacities for lateral-torsional buckling (M_{be}), local buckling (M_{ol}) and distortional buckling (M_{od}). For all columns, M_b was controlled by lateral-torsional buckling.

Table 1: Critical buckling loads and nominal member moment capacity for column

Test	M_{cr} kNm (kip-ft)	M_b kNm (kip-ft)
1, 2, 3, 4	19.4 (14.3)	19.4 (14.3)
5	26.2 (19.3)	26.1 (19.2)
6	23.4 (17.3)	23.4 (17.3)
7, 8	25.7 (19.0)	25.7 (19.0)

For the capacity in compression, four input values are needed: the elastic compression buckling load N_{oc}, the nominal compression yield capacity N_y as given in Eq 18, and the elastic compression buckling loads N_{ol} and N_{od}, for local and distortional buckling, respectively, as given in Eqs. 19 and 20. The local and distortional buckling stresses for compression, f_{ol} and f_{od}, can be determined through a finite strip analysis with applied compression on the column cross-section through software such as CUFSM (Li & Schafer 2010) and ThinWall (Papangelis & Hancock 1995). The area A is calculated from the measured column dimensions, and f_y is taken as the measured yield stress from the experiments.

$$N_y = Af_y \quad (18)$$

$$N_{ol} = Af_{ol} \quad (19)$$

$$N_{od} = Af_{od} \quad (20)$$

Following the Direct Strength Method for $N_{oc}=(P_{cr})_{Euler}$ and the values determined for f_{ol} and f_{od} from a finite strip analysis with the measured column dimensions, the member compression capacity, N_c, is calculated. N_c is the minimum of the member compression capacities for flexural, torsional or flexural-torsional buckling (N_{ce}), local buckling (N_{cl}) and distortional buckling (N_{cd}). For the specific column analyzed N_c=267 kN, and was controlled by local buckling.

3. Internal Actions

3.1 Calibration of FEM

A finite element model (Fig. 3) was created in MASTAN2 (McGuire et al. 2000) composed of 2D beam elements, as is common practice in industry, to determine internal actions of the column. The dimensions of the model were the centerline dimensions of the test frame, and measured dimensions of the cross section and material properties were utilized. Column base springs were included in the model and had the average base stiffness for all experiments with applied vertical loading only, or with the spring stiffness matching each experiment for applied wind and vertical loading, as given elsewhere (Blum & Rasmussen 2016b; Blum & Rasmussen 2016c). Previous studies have determined that the column base stiffness had a large impact on frame ultimate load when wind loading was considered, but not for applied vertical loads only (Blum & Rasmussen 2016e). Connections between the column to rafter, knee to column, and knee to rafter were pinned. Because of the effective triangle formed between the knee, column, and rafter at the eaves connection, the true spring stiffness of the eaves connection had minimal impact. However, the effect of the in-plane bending stiffness of the apex connection had to be investigated.

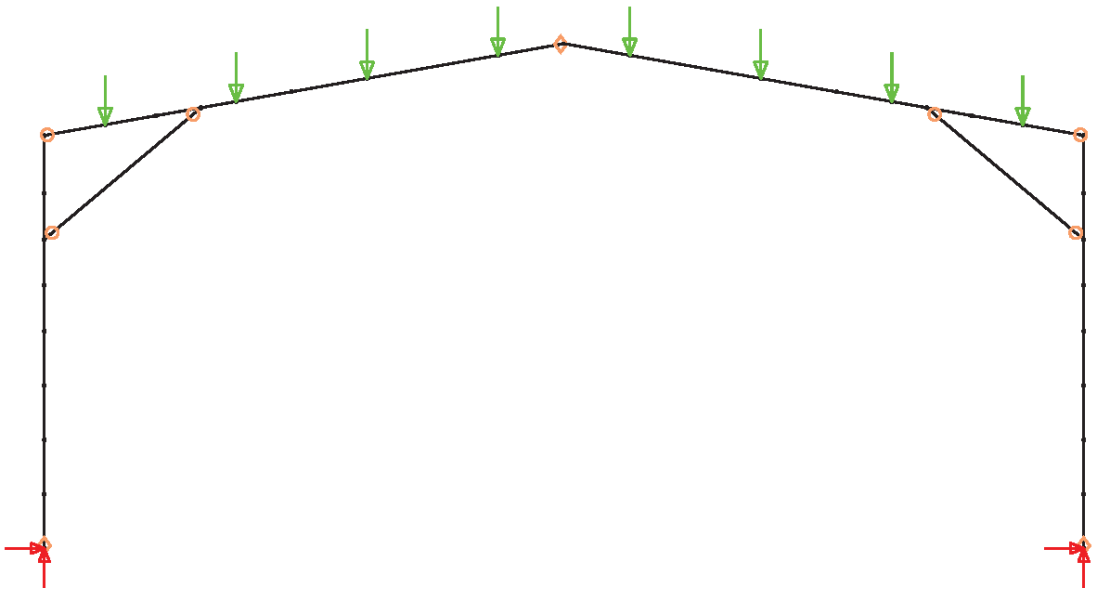

Figure 3: Beam element model of portal frame

A total of 24 kN (5.4 kip) vertical load was applied to the beam element model, and a second order elastic analysis was completed, for various apex spring stiffness values. The maximum bending moment in the column, which occurs at the knee connection, was recorded for each case. A plot of the maximum column moment for each apex stiffness value is shown in Fig. 4. A pinned apex connection results in a 24.1 kNm (17.8 kip-ft) maximum bending moment in the column, while a fixed apex connection has a maximum column bending moment of 18.9 kNm (13.9 kip-ft), which is a 21.6% decrease. Increasing the apex stiffness from pinned up to a stiffness of approximately 35 kNm/deg (25.8 kip-ft/deg) results in a sharp decrease in the maximum column moment. Therefore, the apex connection stiffness must be determined to produce a beam element model which accurately determines the frame bending moments.

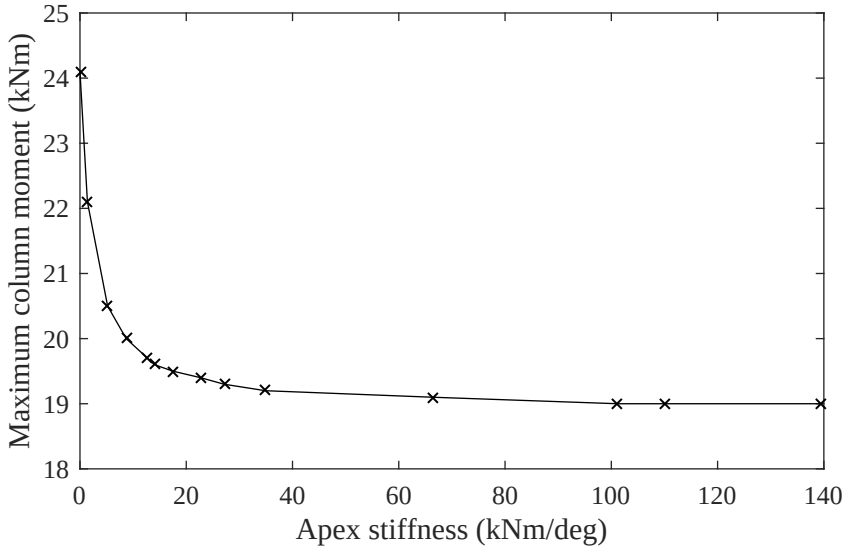

Figure 4: Maximum column bending moment vs. apex stiffness

In lieu of experimental data on the apex connection stiffness, the apex connection was modeled with shell elements in ABAQUS (ABAQUS 2014) to determine an apex spring stiffness to incorporate in a beam element model. The apex model included the apex brackets and 664 mm (26.1 in) long sections of the rafter, as shown in Fig. 5. These rafter sections were long enough to replicate the bending moment at the apex connection in the full frame tests, but short enough to limit the effects of rafter bending. The ends of the rafters were connected to a thick plate using a surface-to-surface tie constraint, and the plates were defined as rigid bodies. Boundary conditions were applied to the end plates at rigid body reference nodes to prevent movement vertically and out-of-plane. Out-of-plane restraints were applied to the rafters at the locations of the purlin brackets, and at the center of the apex bracket. A horizontal restraint was applied at the center of the apex bracket to prevent rigid body motion. Bolts connecting the apex brackets to the rafters were modeled as described elsewhere (Blum & Rasmussen 2016e). Moments were applied to the rigid body reference nodes to load the connection in bending. Downward deflections were recorded at the centerline of the rafters for a 100 mm (3.94 in) length starting at the end of the apex brackets. The starting point was chosen to avoid local effects of the connection, and the 100 mm length was chosen to be long enough to obtain a characteristic rotation while short enough to limit the effects of rafter bending. The deviation of the recorded deflections from the assumed deflections of a fully rigid connection is the rotation of the apex

connection. The rotations from each side of the connection were combined to determine a moment-rotation relationship for the entire apex connection, and is shown in Fig. 6.

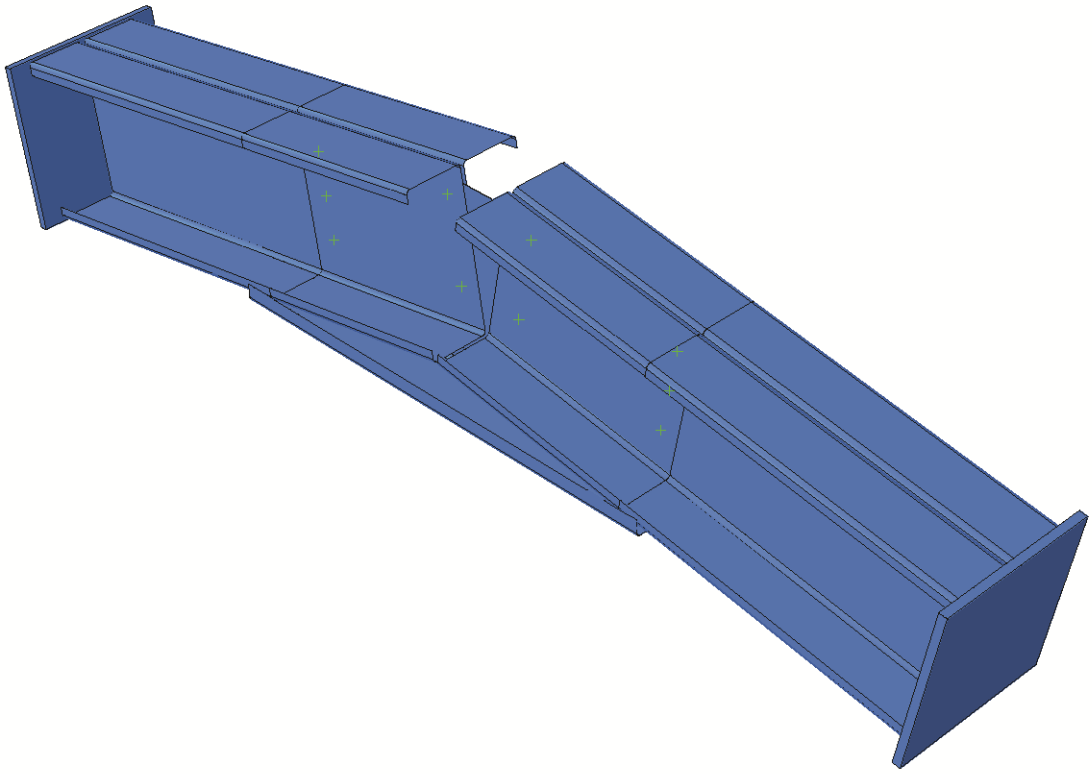

Figure 5: Model of apex connection used to determine apex stiffness

The moment-rotation relationship of the apex connection is essentially linear up to an applied moment of 18 kNm (13.3 kip-ft). No failure was observed in the apex connections during the full scale experiments. Therefore, it is assumed that the connection remained in the elastic range during the experiments and consequently the elastic stiffness was used in the beam element models. A linear regression was fitted though the elastic region of the moment-rotation plot of the apex connection, and the resulting spring stiffness was determined to be 27 kNm/deg (19.9 kip-ft/deg).

The apex spring was added to the beam element model, and a second order analysis was completed. The apex vertical deflection was recorded and compared to the load versus apex vertical deflections for the experiments with applied vertical load only. The model with the apex spring (k=27 kNm/deg) had fairly good agreement with the experiments, especially in the vicinity of ultimate loads. (The apex stiffness determined from the ABAQUS model assumed no bolt-slip in the connection. Bolt holes were sized 2 mm (0.08 in) in diameter larger than the diameter of the bolt. The theoretical rotation due to maximum bolt slip could be calculated and used to determine a reduced apex connection stiffness. However, the effects of bolt-slip were not evident in the experiments, a reduced apex stiffness would not result in an improved match to the experimental data. Therefore, the apex stiffness of 27 kNm/deg was determined to be suitable for use in the beam element model).

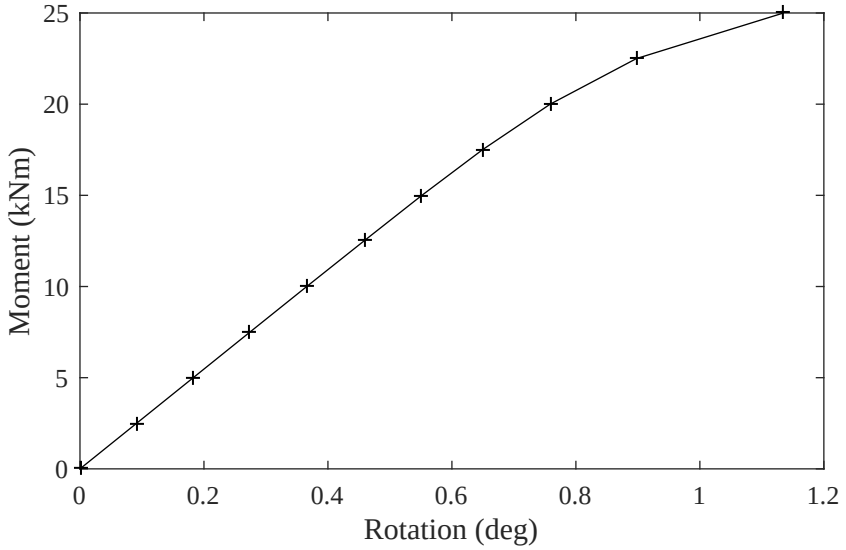

Figure 6: Moment vs. rotation of apex stiffness from the finite element model

3.2 Notional Horizontal Forces

Notional horizontal forces are used in the analysis of nominally perfect rectangular frames to consider the effects of initial frame sway (Ziemian 2010). If the frame has an initial sway and the column of length L is out-of-plumb a distance of x, a horizontal load equal to the applied vertical load at each frame level multiplied by the notional load coefficient of x/L can be applied to the nominally perfect frame. It has been shown that the notional horizontal force applied to the nominally perfect rectangular frame causes the same deflections as a rectangular frame with an initial sway and no notional horizontal force (Ziemian 2010). To test if this same method could be applied to haunched portal frames, two models in MASTAN2 were created, one with nominal frame dimensions and a notional horizontal force applied at the eave equal to 1/310 of the vertical load, and another model with an initial frame sway equal to L/310 and vertical load only. Both frames had the same column base stiffness (equal to the average base stiffness for all experiments), a rigid apex connection, and pinned connections at the eaves and knee brace to column and rafter connections. A vertical load of 28 kN (6.3 kip) was applied at the nodal locations shown in Fig. 3 to both models, and the vertical deflections at the apex and horizontal deflections at the eaves were recorded at various load increments. There was a 0.1% difference in apex vertical deflections between the two models, and a 0.09% difference in eaves horizontal deflections. Therefore, the same notional horizontal load method used for rectangular frames can be applied towards haunched portal frames, and is shown in Fig. 7.

Notional loads were included in the 2D frame analysis to represent the effects of initial imperfections in the nominally vertical columns, as specified in various design codes ((AISC 360-10 2010) and (AISI-S100-07 2007)). The AISI standard specifies a notional horizontal load coefficient of 1/240, which is based on measured out-of-plumb data of cold-formed steel storage racks (Sarawit & Pekoz 2007). The AISC standard specifies a notional load coefficient of 1/500, which represents the maximum tolerance on column story out-of-plumb. The draft 2016 revision of AS/NZS 4600 includes an appendix on analysis methods, which specifies an initial notional horizontal force of 1/200 with additional reduction factors dependent on the height of the columns and the number of columns in a row. For the frame system tested in the accompanying

experiments (Blum & Rasmussen 2016c; Blum & Rasmussen 2016d), the horizontal notional load coefficient is calculated as 1/270 according to the draft revision of AS/NZS 4600. Alternatively, the horizontal notional load can be determined based on measured frame imperfection data from the experiments. The average frame sway, which was previously measured from the experiments (Blum & Rasmussen 2016c), is $L/310$, and therefore a horizontal notional load coefficient of 1/310 was applied to the model.

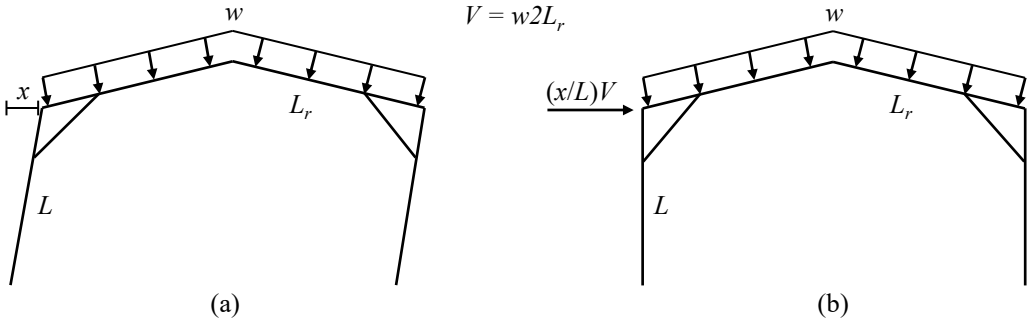

Figure 7: Notional load model (a) frame with column sway x, and (b) straight frame with notional horizontal load

3.3 Determination of Internal Actions

The notional horizontal load was applied at the eave connection between the column and apex on one column to produce a destabilizing effect. A second-order elastic analysis was performed. The internal actions of bending moment and compression on the column at the knee connection were recorded, as this was the location of maximum bending moment. The bending moment distribution along the column was similar for frames with applied wind and vertical loads as those with vertical loads only. Therefore, for wind loaded frames, the 5 kN (1.1 kip) wind load was applied to the model at the eave connection in addition to the notional horizontal force and the vertical loads, and the internal actions of the column at the knee connections were recorded.

4. Design Procedure and Results

The columns are designed as beam-columns as they support large bending moments. For combined axial compression and bending about the x-axis, the interaction equation shown in Eq. 21 is utilized to calculate the column capacity. The member capacities M_{bx} and N_c were calculated using the Direct Strength Method outlined in Section 2.3. The capacity reduction factors for bending, ϕ_b, and for members in compression, ϕ_c, were taken as 1.0 since measured section and material properties were considered, and thus reduction factors to account for the variability of section and material properties were not required. The internal actions M_x* and N* were determined from the 2D finite element model for various load levels. The applied vertical load at which Eq. 21 holds true is the capacity of that frame, as the columns were the critical members and failed before the rafters or knee braces.

$$\frac{N^*}{\phi_c N_c} + \frac{M_x^*}{\phi_b M_{bx}} = 1 \tag{21}$$

The frame capacity for all experiments was determined by this method and the results are presented in Table 2. Overall, the design capacity slightly overestimates the experimental frame ultimate vertical load, with a maximum overestimation of 7.94%. The frame in experiment 3 was

significantly stronger than predicted. It is not obvious what caused the strength increase for that frame, as the ultimate vertical load for experiment 3 was greater than a frame with fully rigid bases, as specified elsewhere (Blum & Rasmussen 2016e). Therefore, that experiment can be considered an outlier. At frame capacity, the bending moment term of the interaction equation is equal to 0.96, which indicates that the column capacity is strongly dominated by bending. The energy method approach provides an upper bound for column buckling loads, and becomes more accurate with more precise displacement fields used in the analysis. The displacement fields given in Eqs. 9 and 10 were determined from four measured displacements along the column height, and were therefore not exact displacement fields. Column buckling loads calculated with the energy method approach overestimated the experimental column buckling loads within 10% (Blum & Rasmussen 2016a). This buckling load was then used in the Direct Strength Method to calculate the capacity of the column, and therefore the overestimation of the column buckling load through the energy method approach contributed to the overestimation of the frame design capacity.

Table 2: Comparison of frame ultimate vertical loads

Test	Experiment kN (kips)	Design Capacity kN (kips)	% Difference
1	21.8 (4.90)	23.0 (5.17)	5.50
2	22.8 (5.13)	23.0 (5.17)	0.88
3	19.5 (4.38)	14.8 (3.33)	-24.1
4	13.3 (2.99)	13.4 (3.01)	0.75
5	29.8 (6.70)	30.2 (6.79)	1.34
6	17.5 (3.93)	18.4 (4.14)	5.14
7	29.8 (6.70)	29.8 (6.70)	0.00
8	18.9 (4.25)	20.4 (4.59)	7.94

In order to produce conservative design capacities, a reliability analysis can be completed to determine the reduction required of M_{cr} from the energy method approach to meet a target reliability index. The method for such an analysis is given in Chapter F "Tests for Special Cases" in the AISI specification (AISI-S100-12 2012) and the equation is presented in Eq. 22 where C_ϕ is the calibration coefficient, M_m, F_m, and P_m are the mean values of the material factor, fabrication factor, and professional factor, respectively, V_M, V_F, and V_P are the coefficients of variation of the material factor, fabrication factor, and professional factor, respectively, C_P is the correlation factor, V_Q is the coefficient of variation of the load effect, and β_o is the target reliability index. The values for C_ϕ and V_Q are given as 1.52 and 0.21 for LRFD, and the values for M_m, V_M, F_m, and V_F are given in Table F of the standard as 1.05, 0.10, 1.00, and 0.05 for a member with combined axial load and bending. P_m and V_P are calculated from the results given in Table 2 as the ratio of tested strength (experimental results) to calculated strength (design capacity). As experiment 3 is considered an outlier, the sample size is n=7 and C_P is calculated as $((1+1/n)(n-1))/(n-3)=1.71$, as given in Chapter F. Resistance factors are given as $\phi_b = 0.90$ for bending and $\phi_c = 0.85$ for compression. There is no designated resistance factor for beam-column members, but as the column in this case is dominated by bending, $\phi = 0.90$ is used. M_{cr} from the energy analysis is reduced and the design procedure outlined previously is followed. From the results, values of P_m and V_P are calculated for each reduction level, and the resulting reliability

index, β, is determined through Eq. 22. The results of the design capacity by reducing M_{cr} by 5% and 10% are shown in Table 3, and the resulting values of P_m, V_P, and β are given in Table 4.

$$\varphi = C_{\varphi}\left(M_m F_m P_m\right) e^{-\beta_o \sqrt{V_M^2 + V_F^2 + C_P V_P^2 + V_Q^2}} \tag{22}$$

Table 3: Design capacity of frames for various M_{cr} reduction levels

Test	Experiment Ultimate Capacity, kN (kip)	Design Capacity, kN (kip)	
		5% M_{cr} reduction	10% M_{cr} reduction
1	21.8 (4.90)	21.8 (4.90)	20.8 (4.68)
2	22.8 (5.13)	21.8 (4.90)	20.8 (4.68)
4	13.3 (2.99)	12.2 (2.74)	11.2 (2.52)
5	29.8 (6.70)	29.0 (6.52)	27.6 (6.20)
6	17.5 (3.93)	17.0 (3.82)	15.9 (3.57)
7	29.8 (6.70)	28.4 (6.38)	27.0 (6.07)
8	18.9 (4.25)	19.1 (4.29)	17.8 (4.00)

The target reliability index for structural members is β_o = 2.5 for LRFD. As shown in Table 4, a 5% reduction in M_{cr} determined from the energy analysis archives this target index. Therefore, the design method outlined herein presents a viable method to determine frame ultimate loads for haunched portal frames with intermediate elastic torsional restraints on the unbraced columns, subject to a 5% reduction on the critical bending moment calculated from the energy analysis.

Table 4: Target reliability index for various M_{cr} reduction levels

% M_{cr} reduction	P_m	V_P	β
0	0.97	0.029	2.25
5	1.03	0.033	2.51
10	1.10	0.041	2.73

5. Conclusions

A method to determine frame ultimate vertical loads for haunched portal frames with an intermediate elastic torsional restraint on the unbraced columns was presented. The column capacity was determined through an energy method approach to determine the critical bending moment in the column and was then used in the Direct Strength Method provided in cold-formed steel design codes (AISI-S100-12 2012; AS/NZS 4600 2005). This method does not require the determination of effective length factors, which can be difficult to quantify due to the semi-rigidity of the column bases and the partial torsional restraint at the knee connection. Column internal actions were determined through a 2D beam finite element model which was calibrated with column base stiffness data obtained from experiments and was validated with frame experimental results. It was shown that the notional horizontal force method used for rectangular portal frames is applicable to haunched portal frames as well. As the energy method typically overestimates the column buckling load, a reliability analysis was completed, and it was determined that a 5% reduction of the critical bending moment calculated from the energy analysis is required to achieve a target reliability index of 2.5 for members. Therefore, the design method presented herein is a suitable method to calculate frame ultimate vertical loads for haunched portal frames with an intermediate elastic torsional restraint on the unbraced columns.

Acknowledgments

This research was supported by the Australian Research Council under Linkage Grant LP120200528. A supplementary scholarship provided to the first author by the Centre for Advanced Engineering at the University of Sydney is gratefully acknowledged. The authors would also like to thank BlueScope Lysaght for providing testing materials.

References

ABAQUS, 2014. ABAQUS / Standard Version 6.14.

AISC 360-10, 2010. *Specification for Structural Steel Buildings*, Chicago, Illinois: American Institute of Steel Construction.

AISI-S100-07, 2007. *North American Specification for the Design of Cold-formed Steel Structural Members*, Washington, D.C.: American Iron and Steel Institute (AISI).

AISI-S100-12, 2012. *North American Specification for the Design of Cold-formed Steel Structural Members*, Washington, D.C.: American Iron and Steel Institute (AISI).

AS/NZS 4600, 2005. *Australian Standard AS/NZS 4600:2005 Cold-formed steel structures*, Sydney, NSW, Australia: Standards Australia.

ASI, 2014. *Design Guide Portal Frame Steel Sheds and Garages*, Australian Steel Institute.

Blum, H.B., 2017. *Long-Span Cold-Formed Steel Portal Frames Composed of Double Channels*. PhD Thesis. The University of Sydney.

Blum, H.B. & Rasmussen, K.J.R., 2016a. Buckling and design of columns with intermediate elastic torsional restraint. In *Proceedings of the Annual Stability Conference*. Orlando, Florida.

Blum, H.B. & Rasmussen, K.J.R., 2016b. Experiments on column base stiffness of long-span cold-formed steel portal frames composed of double channels. In *Proceedings Twentythird International Speciality Conference on Cold-Formed Steel Structures*. Baltimore, Maryland.

Blum, H.B. & Rasmussen, K.J.R., 2016c. Experiments on long-span cold-formed steel double-channel portal frames. In *Research Report No R962, Centre for Advanced Structural Engineering*. Sydney, NSW, Australia: School of Civil Engineering, The University of Sydney.

Blum, H.B. & Rasmussen, K.J.R., 2016d. Experiments on long-span cold-formed steel portal frames composed of double channels. In *Proceedings of the Seventh International Conference of Coupled Instabilities in Metal Structures*. Baltimore, Maryland.

Blum, H.B. & Rasmussen, K.J.R., 2016e. Finite element modeling and parametric study of cold-formed steel portal frames. In *Proceedings SEMC Conference*. Cape Town, South Africa.

ECCS, 2008. *Worked examples according to EN1993-1-3*, Brussels, Belgium: European Convention for Constructional Steelwork.

Ings, B.N.L. & Trahair, N.S., 1987. Beam and Column Buckling Under Directed Loading. *Journal of Structural Engineering, ASCE*, 113(6), pp.1251–1263.

Li, Z. & Schafer, B.W., 2010. Buckling analysis of cold-formed steel members with general boundary conditions using CUFSM: Conventional and constrained finite strip methods. In *Proceedings Twentieth International Speciality Conference on Cold-Formed Steel Structures*. pp. 17–31.

McGuire, W., Gallagher, R.H. & Ziemian, R.D., 2000. *Matrix Structural Analysis*, New York City: John Wiley & Sons, Inc.

Papangelis, J.P. & Hancock, G.J., 1995. Computer Analysis of Thin-Walled Structural Members. *Computers and Structures*, 56(1), pp.157–176.

Sarawit, A.T. & Pekoz, T., 2007. Notional load method for industrial steel storage racks. *Thin-Walled Structures*, 44(12), pp.1280–1286.

Schafer, B.W., 2006. Designing Cold-Formed Steel Using the Direct Strength Method. In *Proceedings Eighteenth International Speciality Conference on Cold-Formed Steel Structures*. Orlando, Florida, pp. 475–489.

Timoshenko, S.P. & Gere, J.M., 1989. *Theory of Elastic Stability* 2nd ed., McGraw Hill Book Company.

Ziemian, R.D. ed., 2010. *Guide To Stability Design Criteria for Metal Structures* 6th ed., Hoboken, New Jersey: John Wiley & Sons, Inc.